Probabilistic Modeling of Rosette Formation

Mian Long,* Juan Chen,* Ning Jiang,† Periasamy Selvaraj,‡ Rodger P. McEver,§¶ and Cheng Zhu†
*National Microgravity Laboratory, Institute of Mechanics, Chinese Academy of Sciences, Beijing 100080, People's Republic of China; †Coulter Department of Biomedical Engineering, Georgia Institute of Technology, Atlanta, Georgia 30332; ‡Department of Pathology and Laboratory Medicine, Emory University School of Medicine, Atlanta, Georgia 30322; and §Cardiovascular Biology Research Program, Oklahoma Medical Research Foundation, and ¶Department of Biochemistry and Molecular Biology and Oklahoma Center for Medical Glycobiology, University of Oklahoma Health Sciences Center, Oklahoma City, Oklahoma 73104

ABSTRACT Rosetting, or forming a cell aggregate between a single target nucleated cell and a number of red blood cells (RBCs), is a simple assay for cell adhesion mediated by specific receptor-ligand interaction. For example, rosette formation between sheep RBC and human lymphocytes has been used to differentiate T cells from B cells. Rosetting assay is commonly used to determine the interaction of Fc γ-receptors (FcγR) expressed on inflammatory cells and IgG coated on RBCs. Despite its wide use in measuring cell adhesion, the biophysical parameters of rosette formation have not been well characterized. Here we developed a probabilistic model to describe the distribution of rosette sizes, which is Poissonian. The average rosette size is predicted to be proportional to the apparent two-dimensional binding affinity of the interacting receptor-ligand pair and their site densities. The model has been supported by experiments of rosettes mediated by four molecular interactions: FcγRIII interacting with IgG, T cell receptor and coreceptor CD8 interacting with antigen peptide presented by major histocompatibility molecule, P-selectin interacting with P-selectin glycoprotein ligand 1 (PSGL-1), and L-selectin interacting with PSGL-1. The latter two are structurally similar and are different from the former two. Fitting the model to data enabled us to evaluate the apparent effective two-dimensional binding affinity of the interacting molecular pairs: 7.19×10^{-5} μm^4 for FcγRIII-IgG interaction, 4.66×10^{-3} μm^4 for P-selectin-PSGL-1 interaction, and 0.94×10^{-3} μm^4 for L-selectin-PSGL-1 interaction. These results elucidate the biophysical mechanism of rosette formation and enable it to become a semiquantitative assay that relates the rosette size to the effective affinity for receptor-ligand binding.

INTRODUCTION

Rosetting is an immunological assay for a receptor-expressing target nucleated cell to form aggregates with ligand-coated erythrocytes, or red blood cells (RBCs) (1,2). In a typical rosetting procedure, cells are mixed at a ratio of 100 RBCs per target cell (1). After incubation, the cells are inspected visually using a hemocytometer. A rosette is defined as a target cell bound with a given number (usually three) or more of RBCs. The percentage, or fraction, of target cells that form rosettes is reported as a metric for the extent of adhesion mediated by the specific receptor-ligand interaction in question. Before the advent of lymphocyte specific monoclonal antibodies (mAbs), rosetting was used to fractionate subpopulations of cells such as thymocytes and bone marrow cells in the early 1970s (2). Many erythrocyte species, including sheep and human, were tested for their ability to form rosettes with T cells. Rosetting with sheep RBCs has been used to differentiate human T lymphocytes from B lymphocytes, because T cells, but not B cells, express receptor CD2, which binds counter-receptor CD58 that is expressed on sheep RBCs (1,2). Human RBCs form rosettes with activated T cells but not with naïve T cells, because CD58 is expressed on human RBCs at a lower level than on sheep RBCs and CD2 expression is low on naïve T cells but is upregulated by activation (1,3).

Because of its dependence on the specific interactions of receptors and ligands and on their expression levels, rosetting has been used as a simple assay for receptor-mediated cell adhesion (1). Apart from classical adhesion receptors, rosetting assay has also been widely used in measuring the functional state of Fc γ-receptors (FcγRs), because the adhesion of FcγRs-expressing inflammatory cells to antibody-coated target cells is a prerequisite for initiation of FcγR-mediated effector functions such as antibody-dependent cellular cytotoxicity and phagocytosis (4,5). However, rosetting has not been regarded as a quantitative method in spite of these routine uses by immunologists for functional assays. The reason is that the measured rosette fraction has not been quantitatively related to the molecular properties of the interacting receptors and ligands.

Thus, a mathematical model that describes rosette formation in terms of the molecular properties can turn rosetting into a more quantitative assay. This model has to account for the observation that rosetting is nondeterministic, as it always results in a mixed population of target cells bound with variable numbers of RBCs, or variable rosette sizes, that range from none to 10 some RBCs per target cell. To introduce randomness in the mathematical description for the size of any particular rosette, an early model assumed heterogeneity in the binding affinity of the interacting receptors and ligands (6). The same assumption was used in a later model (7). This assumption does not seem valid, as receptor-ligand binding

Submitted February 8, 2006, and accepted for publication March 17, 2006.

Address reprint requests to: Dr. Mian Long, National Microgravity Laboratory, Institute of Mechanics, Chinese Academy of Sciences, Beijing 100080, People's Republic of China. Tel.: 86-10-6261-3540; Fax: 86-10-6261-3540; E-mail: mlong@imech.ac.cn.

© 2006 by the Biophysical Society

0006-3495/06/07/352/12 $2.00

doi: 10.1529/biophysj.106.082909

affinity is an intrinsic property of the interacting molecular pair, and as such, should not vary from cell to cell in a population. Neither model has been tested experimentally.

More recently, we have developed a series of mathematical models for treatment of adhesion mediated by a low number of receptor-ligand bonds (8–12). A key feature of this type of adhesions is their weakness, such that whether adhesion occurs becomes random, thereby requiring a probability to describe the likelihood of its occurrence. We solved the probability of adhesion in terms of the densities of the receptors and ligands as well as their binding affinity (8–12). Here, we extended this approach to model the rosetting assay, which results in a Poisson distribution for rosette sizes. Experimental tests of the mathematical model were performed using RBCs coated with multiple densities of IgG- or selectin rosetting, respectively, with nucleated cells expressing multiple levels of FcγRIII (CD16) or selectin ligand. Rosette formation was shown to be initiated by low number of weak IgG-FcγR or selectin-ligand bonds, followed by a stabilizing step that enables the rosettes to survive the lengthy handling process. Apparent binding affinities were evaluated from fitting the Poisson distributions to the measured rosette size histograms or the rosetting fractions. These provided strong support for the validity of our model.

MODEL DEVELOPMENT

The starting point of our mathematical model is the probability of adhesion, P_a, which is a measure of the likelihood for a receptor-expressing cell to adhere to a ligand-expressing cell when the two are put into contact. For static experiments conducted in the absence of dislodging forces such as the rosetting assay, we have previously shown (8,9) that the probability of no adhesion, $1 - P_a$, decays exponentially with increasing densities of the receptors (m_r) and ligands (m_l) as well as their binding affinity (K_a), such that

$$P_a = 1 - \exp(-m_r m_l A_c K_a), \tag{1a}$$

where A_c is the contact area. An implicit simplifying assumption for Eq. 1a is that the adhesion is mediated by a single species of receptor-ligand pair and their binding is a single-step second-order forward and first-order reverse reaction. More involved kinetic mechanisms can be similarly modeled, including multi-valent, multi-species, and multi-step binding as well as the combinations thereof. For example, the adhesion probability for a single-step reversible reaction of ν_r receptors binding to ν_l ligands to form ν_b bonds can be expressed by (9)

$$P_a = 1 - \left[\sum_{m=0}^{\infty} (m_r^{\nu_r} m_l^{\nu_l} A_c^{\nu_b} K_a)^m / (m!)^{\nu_b}\right]^{-1}. \tag{1b}$$

The adhesion probability for the concurrent but independent binding of two distinct receptor species (of respective surface densities m_{r1} and m_{r2}) to their corresponding ligands (of respective surface densities m_{l1} and m_{l2}) can be expressed by (11)

$$P_a = 1 - \exp(-m_{r1} m_{l1} A_c K_{a1} - m_{r2} m_{l2} A_c K_{a2}), \tag{1c}$$

where K_{ai} ($i = 1, 2$) are the respective binding affinities for the two species. The adhesion probability for a two-step reaction consisting of a second-order forward and first-order reverse process in the first step and a first-order forward and first-order reverse process in the second-step can be expressed by (see Appendix)

$$P_a = 1 - \exp[-m_r m_l A_c K_{a1}(1 + K_{a2})]. \tag{1d}$$

Here K_{ai} are the respective binding affinities for the two steps. Setting $\nu_r = \nu_l = \nu_b = 1$ in Eq. 1b, $m_{r2} = 0$, $m_{l2} = 0$ or $K_{a2} = 0$ in Eq. 1c, and $K_{a2} = 0$ in Eq. 1d reduce Eq. 1b–d, to Eq. 1a, as expected.

For cells in suspension, it is reasonable to assume uniform distributions of receptors and ligands on their surfaces. Our previous experiments (9,13–17) suggest that binding of a ligand-coated RBC to one region of the receptor expressing target cell surface does not affect the ability of another RBC to adhere to another surface region on the same target cell, as long as the two RBCs do not sterically hinder one another, since the ligands on the two RBCs do not compete for the same subpopulation of receptors on the target cell. Since the RBCs greatly outnumber the target cells during mixing, each target cell should have equal opportunity to make contact with as many RBCs as allowable by the geometric constraint. Let N be the maximum number of RBCs that are geometrically possible to simultaneously contact with a target nucleated cell ($N \sim 12$–30, depending on the size of the target cell relative to that of the RBC) (1). Each of these N contacts should be independent and have an equal probability P_a to adhere and an equal probability $1 - P_a$ not to adhere. The probability of having n ($n = 0, 1, \ldots, N$) RBCs to simultaneously adhere to a target cell (called the size of a rosette) therefore obeys a binomial distribution:

$$p_n = \binom{N}{n} P_a^n (1 - P_a)^{N-n}. \tag{2}$$

The mean rosette size $\langle n \rangle$ can be calculated from Eq. 2, $\langle n \rangle = P_a N$. If $\langle n \rangle / N \ll 1$, Eq. 1 can be linearized

$$P_a = \begin{cases} m_r m_l A_c K_a & \text{for monovalent, single-species, single-step} \\ m_r^{\nu_r} m_l^{\nu_l} A_c^{\nu_b} K_a & \text{for multi-valent, single-species, single-step} \\ m_{r1} m_{l1} A_c K_{a1} + m_{r2} m_{l2} A_c K_{a2} & \text{for monovalent, dual-species, single-step} \\ m_r m_l A_c K_{a1}(1 + K_{a2}) & \text{for monovalent, single-species, two-step} \end{cases} \tag{3}$$

The binomial distribution can be approximated by the Poisson distribution:

$$p_n = \frac{(P_a N)^n}{n!} \exp(-P_a N). \quad (4)$$

This equation describes the size distribution of rosettes in a population.

Results of a rosetting experiment are usually expressed in terms of the rosette fraction, defined as the percentage of rosettes exceeding a certain size,

$$P(n \geq n_c) = \sum_{n=n_c}^{\infty} p_n = 1 - \sum_{n=1}^{n_c-1} \frac{(P_a N)^n}{n!} \exp(-P_a N), \quad (5)$$

where n_c is a predetermined rosette size, e.g., $n_c = 3$. P_a in Eqs. 4 and 5 are given by Eq. 3 or by other expressions appropriate for the kinetic mechanisms in question.

MATERIALS AND METHODS

Cells, antibodies, and proteins

Chinese hamster ovary (CHO) cells transfected to express the NA2 allele of human FcγRIIIb (CD16b^{NA2}) were cultured in the same media as reported in our previous work (4). The expression of CD16b^{NA2} was periodically checked via flow cytometry (FACSCalibur, BD Biosciences, San Jose, CA). Human promyelocytic leukemia (HL-60) cells from ATCC (Rockville, MD) were grown in complete RPMI 1640 media supplemented with 2 mM L-glutamine, 100 U/ml penicillin, 10 μg/ml streptomycin, and 10% fetal bovine serum. HL-60 cells constitutively express P-selectin glycoprotein ligand 1 (PSGL-1), which binds both P- and L-selectin.

Erythrocytes were isolated from whole blood of normal healthy volunteers as previously described (13). Briefly, ~7 ml whole blood was collected by venipuncture into sterile Vacutainers (BD Biosciences) containing EDTA. This was carefully layered over 3 ml of Histopaque 1119 and centrifuged (30 min, 700 $\times$ g, room temperature). The supernatant was removed and the pelleted erythrocytes were washed once in RBC storage solution (EAS45) (18). RBCs were stored aseptically at 4°C in EAS45, at ~20% hematocrit for up to 3 weeks with negligible hemolysis.

Naïve F5 T cells were purified from spleens of F5 T cell receptor (TCR) transgenic mouse using a mouse CD8$^+$ T cell enrichment column (R&D Systems, Minneapolis, MN) and stored in complete RPMI media supplemented with 100 U/ml interleukin-2 at 37°C for up to 3 d.

Anti-CD16 mAb CLBFcgran-1 (mouse immunoglobulin 2a, mIgG2a) (19) and anti-CD58 mAb TS2/9 (mIgG1) (1) have previously been described. Human IgG (hIgG) and mIgG1, FITC-conjugated goat anti-hIgG antibody, FITC-conjugated goat anti-mouse antibody, as well as bovine serum albumin (BSA) were purchased from Sigma Chemical (St. Louis, MO). hIgG serves as a low affinity ligand for CD16b^{NA2}.

Soluble P-selectin construct consisting of the Lec-EGF domains and nine consensus repeats (20), anti-P-selectin blocking (G1) and capturing (S12) mAbs (both mIgG1) (21), as well as anti-PSGL-1 blocking mAb PL1 (mIgG1) (22) have been described previously. Soluble L-selectin construct consisting of the Lec-EGF domains and two consensus repeats (23), and anti-L-selectin blocking mAb DREG56 (24) and capturing mAb CA21 (23) (both mIgG1) were generous gifts from Dr. T. K. Kishimoto (Millennium Pharmaceuticals, Boston, MA). Monomeric botinylated major histocompatibility (MHC) molecules (H-2D^b allele) with a single biotin at the C-terminus were produced by the National Institutes of Health (NIH) Tetramer Facility at Emory University. The MHC molecules were complexed with an agonist peptide (pMHC) from the influenza virus recognized by the F5 TCR (25).

Coupling proteins onto RBCs

A previously described, modified chromium chloride method was used to couple hIgG or capturing mAbs (S12 or CA21) onto the surface of fresh human RBCs (17,26). Coupling efficiency of proteins was examined by flow cytometry, using CD58 that is constitutively expressed on RBCs at a known density as a standard (1). hIgG-coated RBCs were directly used in rosetting experiments with CD16b^{NA2}-transfected CHO cells, whereas capturing mAb-coated RBCs were first incubated with 50–200 ng/ml of respective selectin constructs for 30 min at 4°C before used in rosetting experiments with HL-60 cells.

A biotin-streptavidin coupling method was used to coat the biotinylated pMHC monomers onto the surface of human RBCs. After washing with phosphate-buffered saline (PBS), human RBCs were incubated with Biotin-X-NHS (Calbiochem, San Diego, CA) for 30 min at room temperature according to the manufacturer's instruction. RBCs were washed five times using PBS containing 2 mg/ml BSA. Next, streptavidin (Sigma) was added to the RBCs at a concentration of 0.5 mg/ml. After 30 min incubation, cells were washed to remove nonbound streptavidin. The biotinylated pMHC monomers were then added to RBC for 1 h incubation at room temperature. After washing three times in PBS, the RBCs were directly used in rosetting experiment with naïve T cells and can be stored in EAS45 for several weeks.

Site density determination

Site densities of surface proteins coated on RBCs or expressed on CHO or HL-60 cells were measured using flow cytometry and/or immunoradiometric assay (IRMA). To measure densities of hIgG coated via $CrCl_3$ coupling, RBCs were incubated directly with FITC-conjugated goat anti-hIgG antibody (4.7 equivalent FITC per IgG) at a concentration of 10 μg/ml in 200 μl of FACS buffer (RPMI/5 mM EDTA/1% BSA/0.02% sodium azide) on ice for 40 min. To measure the CD16b^{NA2} or PSGL-1 expression, CHO or HL-60 cells were incubated first with anti-CD16 mAb CLBFcgran-1 or anti-PSGL-1 mAb PL1, and then with FITC-conjugated goat anti-mouse secondary antibody (4.4 equivalent FITC per IgG). After washing, the cells were analyzed by flow cytometry (Fig. 1 *a*, *inset*). The site densities were then calculated by comparing the fluorescence intensities of the cells with those of standard beads (Bangs Labs, Fishers, IN) (9,17) (Fig. 1 *a*). To measure densities of P- or L-selectin coupled by capturing mAb-coated RBCs, one set of RBCs precoated with a range of densities of the relevant capturing mAb (five densities for each selectin) were incubated with FITC-conjugated goat anti-mouse antibody and the fluorescence intensities were measured using flow cytometry as above. Another set of RBCs precoated with the same range of densities of capturing mAb were incubated with the corresponding selectin and their site densities were measured by IRMA (17,20). A calibration curve was obtained for each selectin by plotting the selectin site density against the mean fluorescence intensity of the capturing mAb (Fig. 1 *b*), thereby allowing calculation of the site densities of the selectins from the mean fluorescence intensities of the capturing mAb.

Rosetting assay

A modified rosetting procedure, described in detail previously (1,3), was used in the study presented here. Typically, rosetting requires two types of cells, one of larger size but smaller number and the other of smaller size but larger number. Usually the former (termed target cells) are nucleated cells expressing the receptors, and the latter are RBCs expressing the counter-receptor (or ligands). Here we used several cellular and molecular systems, all of which have previously been described (4,17,25). The first system consisted of transfected CHO cells expressing CD16b^{NA2} rosetting with human RBC coated with hIgG (via $CrCl_3$ coupling). The second system consisted of HL-60 cells expressing PSGL-1 rosetting with RBC coated with recombinant P-selectin or L-selectin constructs coupled by the respective capture mAbs. The third system was composed of naïve F5 T cells expressing TCR and CD8 rosetting with RBC coated with recombinant

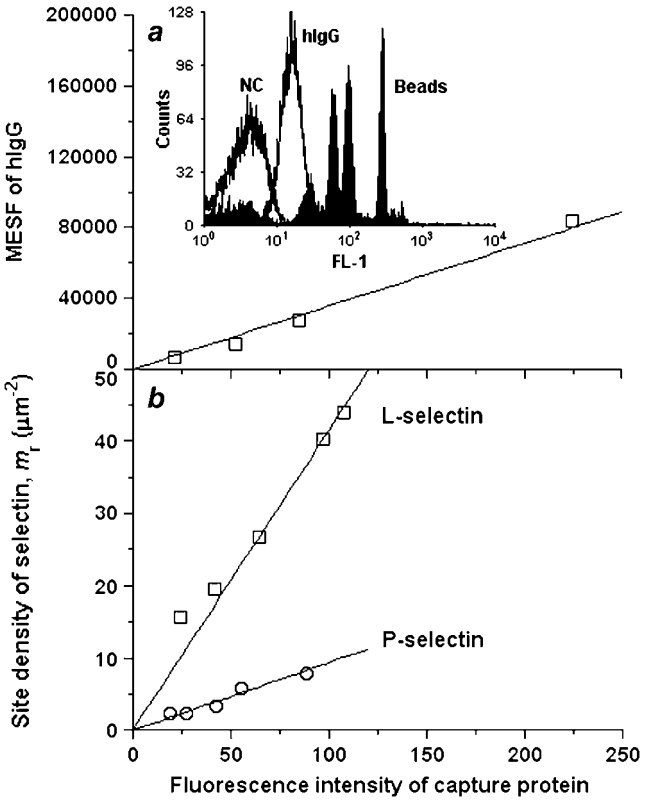

FIGURE 1 Site density determination. (*a*). Flow cytometry was used to determine site density of hIgG coated on RBCs. Calibration curve of standard beads was plotted as molecules of equivalent soluble fluorochromes (MESF) against fluorescence intensity of beads measured by cytometry (*inset*, *solid histograms* labeled *Beads*) using manufacturer-provided program. Fluorescence intensity of coated-hIgG was measured from the cytometry (*inset*, *open histogram* labeled *hIgG*) and the site density was estimated from calibration curve of standard beads after subtracting negative control (*inset*, *open histogram* labeled *NC*). (*b*) Combined immunoradiometric and flow cytometry assays were employed to determine site densities of selectins captured by mAbs precoated on RBCs. Calibration curve was plotted as site density of P- or L-selectin, determined using an IRMA, against fluorescence intensity of capture mAbs (S12 or CA21), measured using flow cytometry assay. Data for P- (*open circles*) and L-selectin (*open squares*) were respectively fitted with straight lines (*solid lines*).

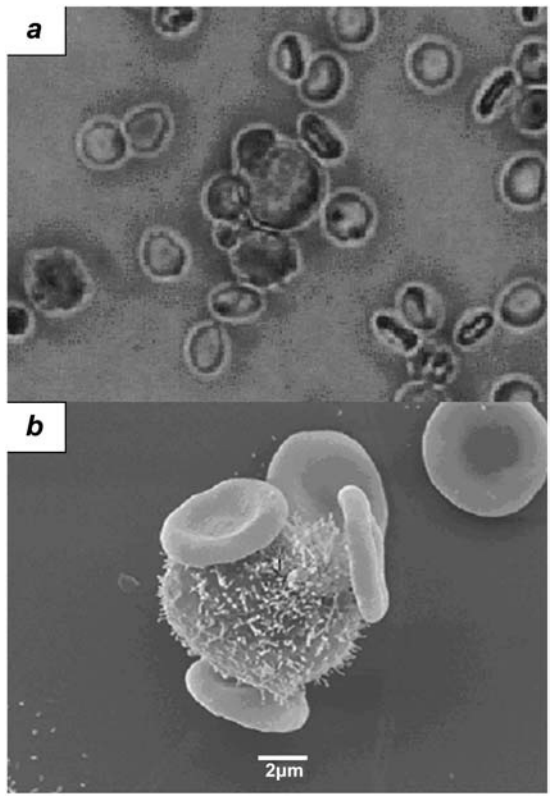

FIGURE 2 Photomicrographs of light microscopic image (*a*) and scanning electron microscopic image (*b*) of a HL-60 cell rosetting with human red blood cells.

pMHC constructs. Cells were washed with RPMI 1640 plus 5% IgG-free serum, mixed at a ratio of 100 RBCs per target cell in total volume of 200 μl, centrifuged at 500 rpm for 5 min or sedimented under gravity without centrifugation (CHO or HL-60 cells) or centrifuged at 1000 rpm for 1 min (T cells), and incubated on ice over 2 h or at room temperature for indicated time. The cell pellet was gently resuspended with 10–15 times of pipetting, and the rosettes so formed were visualized under a light microscope or a scanning electron microscope (Fig. 2, *a* and *b*). More than 300 target CHO or HL-60 cells or 100 T cells were counted within 10 min for each condition in each run of rosetting assay to ensure stable distribution of rosette sizes. All assays were performed in at least duplicate.

Data analysis

To test our model, a Poisson distribution (Eq. 4) was fitted to histograms of measured rosette sizes to evaluate the mean rosette size, $\langle n \rangle = P_a N$. The expression for P_a depends on the kinetic mechanism, four of which have been given by Eq. 3. To test the validity of the multi-valent, single-species, and single-step binding model, $\langle n \rangle$ was plotted against the receptor and ligand densities to evaluate ν_r and ν_l. The lumped binding affinity, $A_c K_a N$ (if both m_r and m_l were known and $\nu_b = 1$), or $A_c m_l K_a N$ (if m_r was known and $\nu_l = 1$), was calculated.

RESULTS

Rosette assay is insensitive to handling procedure after stabilization

Rosette formation was quantified by size distribution of rosettes, p_n, as a function of n. A size n rosette is defined as an aggregate of n RBCs adhering simultaneously to a single target cell but not among themselves (Fig. 2, *a* and *b*). For rosette formation to be used as a quantitative assay, it is necessary that the measurements be robust and not significantly affected by a modest variation in the handling procedure, as forces applied to the rosettes during handling are difficult to control and inevitably variable from time to time and from experimenter to experimenter. Very similar rosette size distributions were obtained when the incubation time to allow RBCs to rosette with HL-60 cells was varied between 2 and 6 h and when the number pipetting to resuspend the RBC-CHO rosettes was varied between 5 and

30 times (Fig. 3, *a* and *b*). In addition, consistent rosette size distributions were obtained by three different experimenters (data not shown). These data indicate that the measured rosette size distributions are objective and reliable.

Two more experiments were performed to test the stability of rosette formation over incubation period and during mixing and handling. In the first experiment, HL-60 cells were mixed with P-selectin-coated RBCs. One sample was immediately transferred to a hemocytometer for observation, whereas another sample was centrifuged, incubated, and resuspended, then transferred to the hemocytometer for observation as in the rosetting assay. The latter sample resulted in a mean rosette size of $\langle n \rangle = 0.13$ for P-selectin site density of $m_r = 0.7\ \mu m^{-2}$, consistent with the results summarized in Table 1 obtained using more extensive data (see below). In sharp contrast, essentially no rosettes were observed in the former sample, which was comparable to the nonspecific control. In the second experiment, rosettes formed in the first experiment (from the second sample) were transferred to a micropipette system for direct examination of the adhesion strength between the HL-60 cell and the RBC(s). Rosettes with some of the RBCs stuck to the cover glass were identified, and the HL-60 cells in those rosettes were aspirated by a micropipette, which was then retracted to pull the HL-60 cells away from the RBCs. It was found that the HL-60 cells adhered strongly to the RBCs. In some cases, instead of separating the cells, the pipette retraction actually resulted in membrane tethers extrusion from the cells.

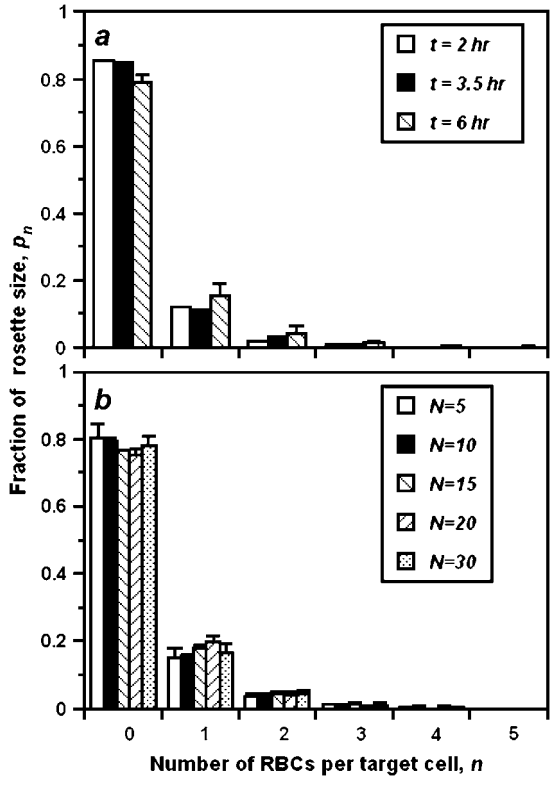

FIGURE 3 Insensitivity of rosette distribution to handling procedure. Rosette size distributions were measured (*a*) when incubation time to allow L-selectin-coated RBCs to rosette with PSGL-1-expressing HL-60 cells was varied from $t = 2$ (*open bars*), 3.5 (*solid bars*), to 6 (*hatched bars*) hr and (*b*) when the number of pipetting to resuspend the rosettes between $CD16b^{NA2}$-transfected CHO cells and hIgG-coated RBCs was changed from $N = 5$ (*open bars*), 10 (*solid bars*), 15 (*rightward-hatched bars*), 20 (*leftward-hatched bars*), to 30 (*dotted bars*) times. Data are presented as the mean ± SD of fraction of rosette sizes in at least duplicate.

Binding is mediated by specific receptor-ligand interactions

Binding was quantified by the mean rosette size, $\langle n \rangle$, which was estimated by fitting the Poisson distribution (Eq. 4) to the histograms of measured rosette sizes (see Figs. 5 and 6). Rosettes were formed between $CD16b^{NA2}$-transfected CHO cells and RBCs when the RBCs were coated with hIgG, but was abolished when hIgG ligand was replaced by an irrelevant protein BSA (Fig. 4 *a*). Rosettes were also formed between HL-60 cells and RBCs when the RBCs were coated with appropriate capturing mAbs (S12 or CA21) and incubated with the corresponding soluble P- or L-selectin constructs, but were abrogated when the capturing mAbs were replaced with the isotype-matched irrelevant mIgG1. In addition, rosette formation was blocked by mAbs against P-selectin (G1) and L-selectin (DREG56) (Fig. 4 *b*). These data demonstrated that the observed rosette formation was mediated by the specific interactions between the $CD16b^{NA2}$-hIgG or selectin-PSGL-1 molecules.

TABLE 1 Summary mean rosette size and 2D apparent affinity values

Molecular systems	m_r (μm^{-2})	m_l (μm^{-2})	$\langle n \rangle$	$A_c K_a N$ $\times 10^5$ (μm^4)
$CD16b^{NA2}$-hIgG	1023	20.3	1.65 ± 0.13	7.95 ± 0.63
	1023	10.3	0.59 ± 0.03	5.63 ± 0.30
	1023	6.6	0.25 ± 0.06	3.68 ± 0.87
	115	11.9	0.12 ± 0.01	9.66 ± 2.94
Mean average				6.73 ± 2.62
Molecular systems	m_r (μm^{-2})	m_l (μm^{-2})	$\langle n \rangle$	$A_c K_a N$ $\times 10^3$ (μm^4)
P-selectin-PSGL-1	3.4	21.3	0.23 ± 0.01	3.18 ± 0.11
	1.9	21.3	0.25 ± 0.01	6.12 ± 0.17
	2.2	21.3	0.22 ± 0.01	4.67 ± 0.29
Mean average				4.66 ± 1.47
L-selectin-PSGL-1	10.0	21.3	0.25 ± 0.02	1.16 ± 0.10
	11.7	21.3	0.10 ± 0.00	0.40 ± 0.02
	4.5	21.3	0.12 ± 0.01	1.26 ± 0.05
Mean average				0.94 ± 0.47

The mean rosette size $\langle n \rangle$ was determined by fitting the Poisson distribution (Eq. 4) to the measured rosette histograms (Figs. 5 and 6). The effective 2D apparent affinity multiplied by N ($\approx$12) (1) was calculated from $A_c K_a N = \langle n \rangle / (m_r \times m_l)$.
Data are presented as mean ± S.D.

Rosette size varies randomly and follows a Poisson distribution

Ligand-coated RBCs were allowed to rosette with receptor-expressing target (CHO or HL-60) cells. The sizes of the rosettes (i.e., number of RBCs per target cell) were visualized microscopically, which were then analyzed by histograms (Figs. 5 and 6, *bars*). The random occurrence and variable rosette sizes might result from the heterogeneity of the cells and their expression of the interacting molecules or from the inherent stochastic nature of weak adhesion mediated by small number of bonds. Multiple lines of evidence support the latter cause, i.e., weak and stochastic adhesion as the mechanism for the random rosette size. Increasing the site densities of receptors and ligands reduced the randomness and increased the size of the rosettes. Conversely, as the receptor and/or ligand site densities decreased, the histogram shifted leftward toward smaller rosette sizes (Fig. 5, *a–d*). Small rosette sizes (most frequently no more than two RBCs per target cell) imply low adhesion probabilities because $P_a = \langle n \rangle / N$. Indeed, direct calculation found $\langle n \rangle \sim 0.12$–$1.87$, which were small compared to the maximally allowable rosette size N (≈ 12). Low adhesion probabilities can result from low densities of interacting molecules by virtue of the mass action effect, as expected from Eq. 1. In fact, the site densities used in the rosetting experiments are comparable to those used in our previous micropipette experiments performed using the same cellular and molecular systems, which resulted in similarly low adhesion probabilities (9,13–15,17). These arguments also justify the approximation used in Eq. 3.

An important prediction of the stochastic adhesion hypothesis is the Poisson distribution of the rosette sizes. It is evident that, for all four pairs of CD16b^{NA2}-IgG site densities studied, the measured rosette size histograms (*bars*) were in excellent agreement with the Poisson distributions (*curves*) obtained by using single-parameter fits ($R^2 = 0.93 \sim 1.00$) (Fig. 5, *a–d*) and the fitted mean rosette sizes also agreed very well with the directly calculated $\langle n \rangle$ values, which were quite small ($0.12 \sim 1.65$).

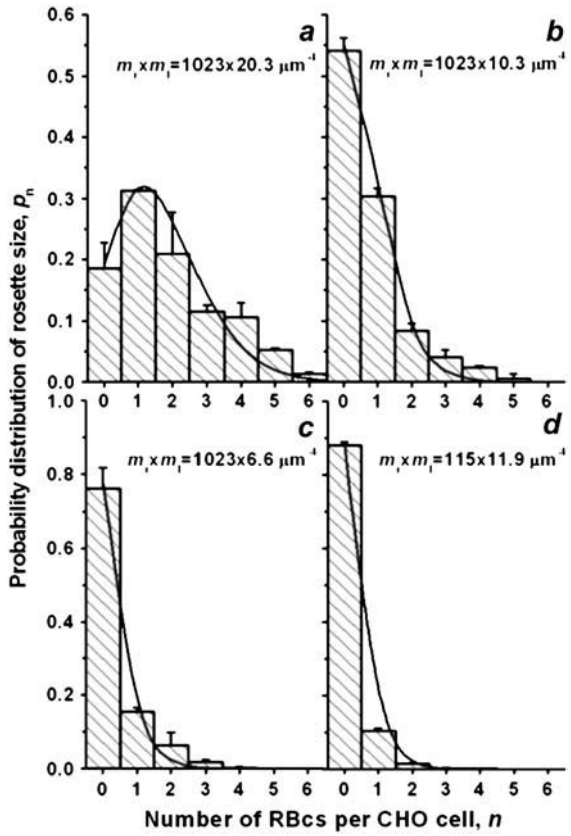

FIGURE 5 Comparison of measured and fitted size distributions of CHO-RBC rosettes mediated by CD16b^{NA2}-hIgG interactions at the site densities of $m_r \times m_l = 1023 \times 20.3$ (*a*), 1023×10.3 (*b*), 1023×6.6 (*c*), and 115×11.9 (*d*) μm^{-4}. Total of >300 CHO cells were counted in each experiment and the measurements were repeated in at least duplicate at each site density. The histograms of rosette sizes (p_n corresponds to the probability of a CHO cell bound with n RBCs, *hatched bars*) were presented as mean ± SD of ≥2 experiments of ≥300 rosette counts for each site density, which was fitted by a Poisson distribution (Eq. 4; *curves*).

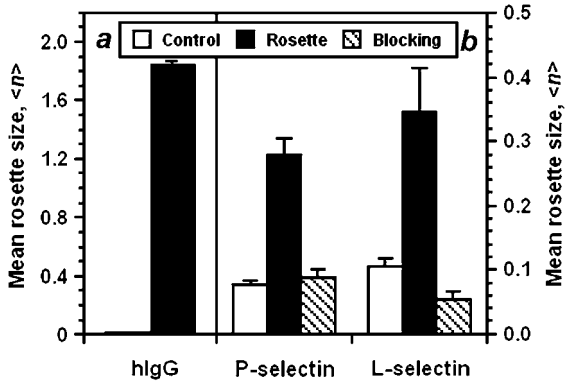

FIGURE 4 Binding specificity. (*a*) CD16b^{NA2}-expressing CHO cells rosetted with hIgG-coated RBCs (*solid bar*). The rosettes were completely abolished by replacing hIgG with BSA (*open bar*). (*b*) Ligand-expressing HL-60 cells respectively rosetted with P- or L-selectin-coated RBCs (*solid bars*). The rosetting was significantly reduced by replacing the capture mAbs with isotype-matched irrelevant mIgG1 (*open bars*) or by incubating with blocking mAbs (*hatched bars*). Data were presented as the mean ± SE of mean rosette size $\langle n \rangle$.

Additional tests were done using RBC-HL-60 cell rosettes mediated by P- or L-selectin interacting with PSGL-1, two molecular systems that are similar to each other structurally and functionally but very different from the CD16b^{NA2}-IgG system. Since the variations in site densities were modest ($m_r = 3.4$, 1.9, and 2.2 μm^{-2} for P-selectin, and $m_r = 10$, 12, and 4.5 μm^{-2} for L-selectin), rosettes measured using three densities for each selectin were pooled together for histogram analysis of their size distributions, which were then fitted by Eq. 4. Again, Poisson distributions (*curves*) fit the data (*bars*) very well (Fig. 6, $R^2 \approx 1.00$) and the fitted mean rosette sizes were also in excellent agreement with the directly calculated small $\langle n \rangle$ values ($0.10 \sim 0.35$).

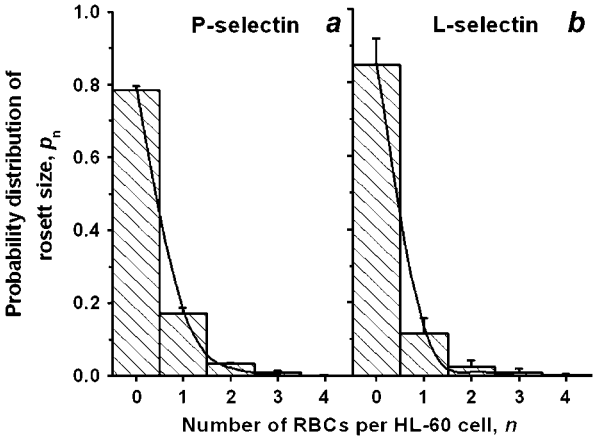

FIGURE 6 Comparison of measured and fitted size distributions of HL-60-RBC rosettes mediated by (*a*) P-selectin-PSGL-1 interactions or (*b*) L-selectin-PSGL-1 interactions. Total of >300 HL-60 cells were counted in each experiment and the measurements were repeated in at least duplicate at each site density. Rosette size histograms (p_n corresponds to the probability of a HL-60 cell bound with *n* RBCs, *hatched bars*) at three site densities for each selectin were lumped together and presented as mean ± SD of ≥10 experiments of ≥300 rosette counts for each selectin, which was fitted by a Poisson distribution (Eq. 4; *curves*).

Dependence of mean rosette size on site densities of receptors and ligands

The kinetic mechanism of an interaction between receptors and ligands can be determined by examining the dependence of adhesion on their site densities, where the site densities were adjusted to avoid the conditions that result in area contact (as opposed to point attachments) mediated by a large number of molecular interactions. To do that we plotted the log of the mean size of rosettes mediated by $CD16b^{NA2}$-IgG interaction against the log of the site densities of receptors (Fig. 7 *a*, *bottom abscissa*) and ligands (Fig. 7 *a*, *top abscissa*). For multi-valent, single-species, and single-step binding, $\langle n\rangle = m_r^{\nu_r} m_l^{\nu_l} A_c^{\nu_b} K_a N$ from Eqs. 3 and 4. The slopes of the linear fits to the data in Fig. 7 *a* represent the stoichiometric coefficients. The values so obtained are $\nu_r \approx 0.7$ and $\nu_l \approx 1.5$, which predicts $\nu_r = \nu_l = \nu_b = 1$ as it is required that the stoichiometric coefficients are integers and $\min(\nu_r,\nu_l) \geq \nu_b \geq 1$. These results confirm the previously determined second-order forward, first-order reverse kinetic mechanism for CD16-IgG interactions (9, 13–15) and provide additional support of our model.

The conclusion regarding the CD16-IgG kinetic mechanism is further supported by the linear appearance of the $\langle n\rangle$ vs. $m_r \times m_l$ plot (Fig. 7 *b*), since $\langle n\rangle = (A_c K_a N) \times (m_r \times m_l)$ from Eqs. 3 and 4 based on the determined stoichiometry. The mean rosette sizes in Fig. 7 *b* were determined using two methods: a), directly calculated from all individually measured rosettes, and b), evaluated by fitting Poisson distributions to the rosette size histograms. The agreement between four sets of values determined by the two methods provides further support of our model (Fig. 7 *b*).

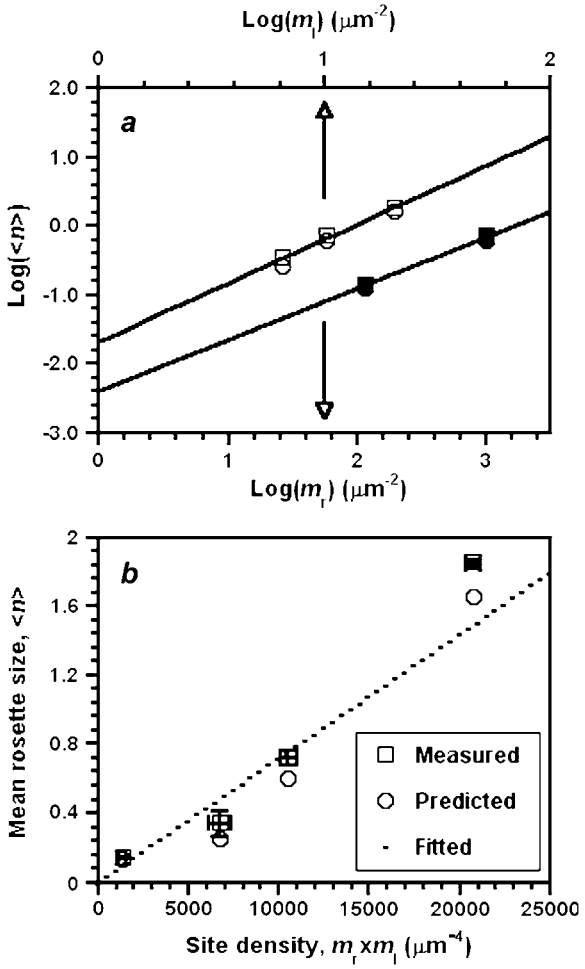

FIGURE 7 Dependence of mean rosette size and independence of apparent binding affinity on site density for CHO-RBC rosettes mediated by $CD16b^{NA2}$-hIgG interactions. (*a*) The log of mean rosette size directly measured (*squares*) and calculated by fitting a Poisson distribution to the rosette size histogram (*circles*) was plotted against the log of receptor (*bottom abscissa*) and ligand (*top abscissa*) densities, which were fitted with straight lines (*lines*) to obtain the stoichiometric coefficients. (*b*) Mean ± SE of rosette size directly measured (*squares*) and calculated by fitting a Poisson distribution to the rosette size histogram (*circles*) was plotted against the product of the densities of receptors and ligands and then fitted by a straight line (*dotted line*). The slope represents the apparent binding affinity (multiplied by the maximally allowable rosette size *N*), $A_c K_a N = 7.19 \times 10^{-5}$ μm^4.

Measuring binding affinity from a quantitative rosette assay

It follows from $\langle n\rangle = (A_c K_a N) \times (m_r \times m_l)$ that the slope of the linear fit to the data in Fig. 7 *b* is equal to the effective two-dimensional (2D) binding affinity, $A_c K_a$, multiplied by the maximally allowable rosette size, *N*. The effective 2D binding affinity (multiplied by *N*) can also be estimated from the mean rosette size determined using a single pair of site densities, i.e., $A_c K_a N = \langle n\rangle/(m_r \times m_l)$. Values of $A_c K_a N$ so determined are summarized in Table 1. As can be seen, consistent values were obtained for the four $CD16b^{NA2}$-IgG

densities. The average A_cK_aN value (6.73×10^{-5} μm^4) is in good agreement with the slope of the linear fit (7.19×10^{-5} μm^4) obtained from Fig. 7 *b*. The ranges of site density variations were too small for P- and L-selectin to produce sufficiently large ranges of mean rosette size variations to allow for robust linear plots. Therefore, the effective 2D binding affinities (multiplied by N) were determined for each site density and the average values were reported in Table 1.

Results of a rosetting assay are commonly reported as rosette fraction, defined as the percentage of target cells that have formed rosettes with RBCs. A rosette is defined as having no less than a predetermined number (n_c) of RBCs bound to a target cell. Effective 2D binding affinity (multiplied by N) can be calculated from the measured rosette fraction using the unity stoichiometric coefficient version of Eqs. 3 and 5. Fig. 8 shows the A_cK_aN values so obtained for the three cellular and molecular systems studied. As can be seen, consistent A_cK_aN values calculated from four different choices of n_c (1, 2, 3, and 4) were obtained for the $CD16b^{NA2}$-IgG system, which are also in excellent agreement with that obtained previously from fitting the Poisson distributions to the rosette size distributions (Fig. 8 *a*), supporting the reliability of estimated binding affinity of $CD16b^{NA2}$-hIgG interactions. Although greater variations in the estimated A_cK_aN values were seen for the selectin systems (Fig. 8 *b*), the results are still deemed acceptable because these can be explained by measurement errors (see Discussion below). Taken together, these results provide strong support for our mathematical model (Eqs. 4 and 5) and have demonstrated that 2D binding affinity can be evaluated from the rosetting assay.

DISCUSSION

Rosette formation is mediated by specific molecular interactions. However, how the receptors and ligands regulate the rosette size distribution through their expression and binding affinity was not quantitatively understood. The goal of the present study was to obtain a quantitative understanding as well as to develop and validate a model that captures such understanding mathematically. The model is based on the probability of adhesion, which was solved from the probabilistic formulation for small system kinetics first proposed by McQuarrie (27). This theory has been developed into a widely applicable framework for mathematical treatment of various cell adhesion experiments including centrifugal detachment (8,28), micropipette adhesion frequency assay (9,13–15,17,29–31), and doublet formation and breakage under flow (10). Here, the theoretical framework has been further extended to describe the rosetting assay. In all cases, the kinetic rates and binding affinity of the specific molecular interactions are the determining parameters of the cell adhesion functions. In the deterministic kinetic framework, the binding affinity determines how many bonds are formed. By comparison, in the present probabilistic kinetic framework, it determines how likely one molecule binds to another. Regardless of the molecular site densities, the Poisson distributions fit the rosetting size histograms well (Figs. 5 and 6). Good agreement was found among binding affinities estimated from experiments using different molecular densities for any of the three interacting molecular pairs studied (Table 1). These results have supported the validity of the model.

The applicability of our model depends on the validity of the assumption that each RBC has equal opportunity to adhere to the same target cell before being sterically hindered by the geometric constraint. To allow easy observation and to increase the sensitivity of the assay, the site densities were adjusted to yield modest mean rosette sizes as shown in Figs. 2–6, which also satisfies the above assumption. High site densities would produce area attachments (as opposed to point attachments) mediated by a large number of molecular interactions and yield large mean rosette sizes. This might be the case in some published studies where the target cells were completed surrounded by RBCs, which likely invalidates the above assumption. Such a case is exemplified in Fig. 9 *a*, where the size distribution of pMHC-coated RBCs rosetting with F5 T cells has a large fraction (>30%) of rosettes having >6 RBCs. It is evident that the measured rosette size distribution (*solid bars* in Fig. 9 *a*) no longer follows the Poisson distribution (*open bars* in Fig. 9 *a*), probably because the effect of steric interactions among adhering RBCs became significant in the large-sized rosettes. Interestingly, after excluding the fractions of rosettes having 0 and >6 RBCs, the renormalized distribution (*solid bars* in Fig. 9 *b*) becomes Poissonian again (*open bars* in Fig. 9 *b*). These data clearly demonstrate how the absence or presence of steric interactions determines whether or not the rosette size follows a Poisson distribution even in different subpopulations of cells assayed in the same experiment. From this comparison, we conclude that steric interactions among

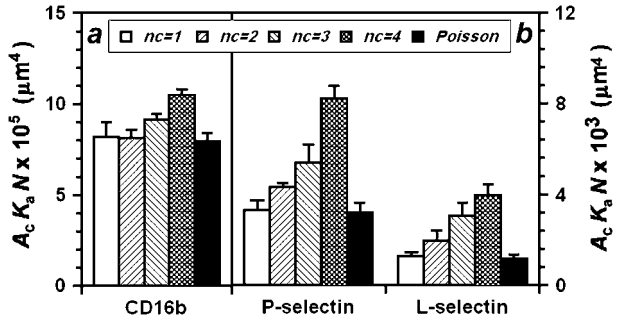

FIGURE 8 Estimation of apparent binding affinity from measurements of CHO-RBC rosettes mediated by $CD16b^{NA2}$-hIgG interactions at $m_r \times m_l = 1023 \times 20.3$ μm^{-4} (*a*) and of HL-60-RBC rosettes mediated by P-selectin at $m_r = 3.4$ μm^{-2} or L-selectin at $m_r = 10$ μm^{-2} interacting with PSGL-1 (*b*). For each system, Eq. 5 was used to calculate the A_cK_aN value from the measured rosette fraction for each of the following preset rosette size, $n_c = 1$ (*open bars*), 2 (*leftward-hatched bars*), 3 (*rightward-hatched bars*), or 4 (*dotted bars*). In addition, the A_cK_aN values were determined by fitting Poisson distributions (Eq. 4) to the rosette size distributions (*solid bars*). Data are presented as the mean ± SE.

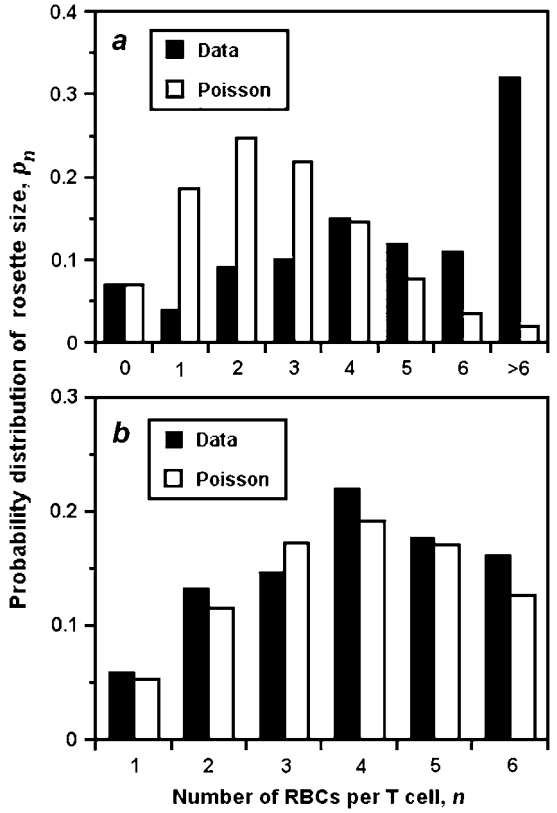

FIGURE 9 Comparisons between the measured size distribution of pMHC coated RBCs rosetting with T cells (*solid bars*) and the Poisson distribution that matches the percentage of rosettes ($n_c \geq 1$) (*open bars*). Data are presented as (*a*) a complete set and (*b*) a subset after exclusion of the fractions of rosettes having 0 and >6 RBCs and renormalization.

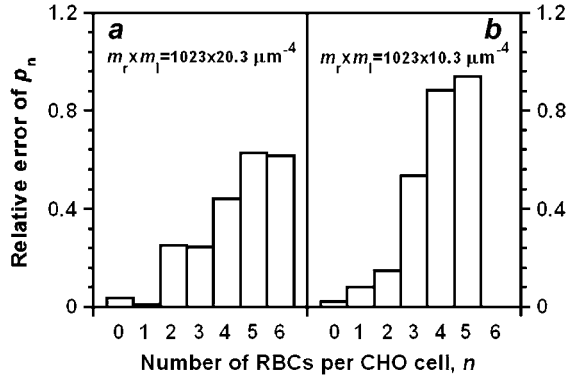

FIGURE 10 The relative errors (absolute values) between measured and fitted rosette size fraction, $|[p_n(\text{measured}) - p_n(\text{fitted})]/p_n(\text{measured})|$, were plotted against the number of RBCs per target cell for CHO-RBC rosettes mediated by CD16b^{NA2}-hIgG interactions at two typical site densities, $m_r \times m_l = 1023 \times 20.3$ (*a*) and $= 1023 \times 10.3$ μm^{-4} (*b*).

adhering RBCs had little adverse impact on the data shown in Fig. 5 *a*, since a), the fraction of six or more adhering RBC is very small (<2%), b), the rosette size distribution is Poissonian, and c), the mean rosette size of Fig. 5 *a* correlates with those in Fig. 5, *b–d*, by the law of mass action (Fig. 7).

The accuracy of the rosette size measurements is determined by several factors, including: a), subjectivity in judging whether a RBC is really attached or merely contiguous to a target cell, b), objectivity of observing a three-dimensional structure from a 2D projection and other observation errors, and c), variation in the experimenter's skill such as breaking up some of the rosettes during resuspending cells before counting. For example, miscounting one RBC in a size n RBC rosette in an experiment that measured 300 target cells would have introduced a $-1/300$ measurement error in the rosette size fraction p_n and a $+1/300$ measurement error in the rosette size fraction p_{n-1}. These errors are trivial when p_n and p_{n-1} are large, but become significant when they are small. This has been exemplified in Fig. 10, where the absolute values of relative errors, $|\Delta p_n/p_n|$, between the fitted Poisson distributions and the measured rosetting size histograms, increase with increasing n (Fig. 10 *b*) when n is negatively correlated with p_n (Fig. 5 *b*). When n is positively correlated with p_n (Fig. 5 *a*, the $n = 0$ and 1 cases), however, $|\Delta p_n/p_n|$ increase with decreasing n (Fig. 10 *a*, the $n = 0$ and 1 cases). Similar results were found for other site densities of the CD16b^{NA2}-hIgG interaction mediated rosettes and for selectin-PSGL-1 interaction mediated rosettes (data not shown). The measurement errors also explain the variations in the selectin-ligand binding affinities estimated using increasing n_c (Fig. 8 *b*). Since n is negatively correlated with p_n in these cases (Fig. 6), the relative error in $P(n \geq n_c)$ would increase with increasing n_c. The binding affinity estimated from the rosetting fraction $P(n \geq 1)$ agrees best with that estimated from fitting the entire Poisson distribution because p_1, which has the smallest relative error, dominates the fitting. The accuracy of the effective 2D affinity values is further limited by that of the measurements of the site densities of the receptors and ligands, which in general are no better than 50%. This explains the fractional slope values of the linear fits to the data in Fig. 7 *a*.

The Poisson distribution of the rosette sizes suggests low adhesion probabilities between the RBC and the target cell, which implies a low number of receptor-ligand bonds. However, this prediction is at odds with the fast kinetic rates of these interactions and their ability to support stable rosette formation over long time. The half-lives (reciprocal off-rates) of bonds of P- and L-selectin interacting with PSGL-1, of CD16b^{NA2} interacting with hIgG, and of F5 TCR interacting with agonist pMHC have been measured using single bond lifetime experiments (32,33) and/or the micropipette adhesion frequency assay (13–17,34), which ranges from a fraction of a second to a few seconds. How could a few of these bonds with such short lifetimes support stable rosettes up to hours and be robust to variations in the handling procedure (Fig. 3)? Although the underlying mechanisms are not clear, the ability of selectin-ligand and FcγR-IgG interactions to mediate static binding has long been observed (8,20,28,35). We hypothesize that the initial

interactions that mediated the rosette formation during centrifugation or sedimentation when the RBCs contacted the target cells were as weak and short-lived as those seen in the micropipette adhesion frequency assay and single bond lifetime assay. However, during incubation, the rosettes were stabilized, because by the time the cell pellet was resuspended, the rosettes were quite stable, as the gentle pipetting that used tips with wide opening would not disrupt them (Fig. 3). This hypothesis was supported by two tests, which showed that immediate re-suspension without incubation did not result in countable rosettes.

The above hypothesis also explains the discrepancies among the effective 2D affinity values for the same selectin-ligand interactions using different experimental methods. The A_cK_a ($= \langle n\rangle/m_rm_lN$) value for the P-selectin-PSGL-1 interaction is 3.9×10^{-4} μm^4 calculated from the $\langle n\rangle$ value in Table 1, which is ~30-fold smaller than the value of 1.2×10^{-2} μm^4 previously estimated by the micropipette adhesion frequency assay using the same HL-60 cells expressing 21.3 PSGL-1 per μm^2 (17). A possible explanation for the discrepancies may be that only a small fraction of the initial weak bonds were able to be converted into strong bonds or to recruit additional bonds, thereby giving rise to much smaller apparent A_cK_a values. For example, the effective 2D affinity for the P-selectin-PSGL-1 interaction estimated from a long-term static sedimentation assay is 4.8×10^{-4} μm^4, which agrees well with the value estimated in this study but much smaller than the value measured by the micropipette (17). As another support of this hypothesis, it was previously noted that the $m_lA_cK_a$ value for E-selectin-ligand interaction estimated from the long-term static centrifugation experiment (8) is an order of magnitude smaller than that estimated by the short-term micropipette adhesion frequency assay (30).

However, an alternative hypothesis may be required to explain the rosettes supported by the $CD16b^{NA2}$-hIgG interaction. The effective 2D affinity for this interaction calculated from the $\langle n\rangle$ value in Table 1 is 5.6×10^{-6} μm^4, which is an order of magnitude larger than the 4.1×10^{-7} μm^4 value previously estimated by the micropipette adhesion frequency assay (14). CD16 is a receptor capable of signaling for immune effector function upon engagement of IgG Fc for sufficiently long time, which may result in higher apparent affinity from a long-term assay than from a short-term assay.

Although elucidation of the stabilization process is beyond the scope of this study, possible mechanisms for apparent changes in the binding characteristics over time may include affinity regulation, e.g., conformational changes that result in higher affinity and slower dissociation (35), avidity regulation, e.g., receptor clustering that result in multimeric bonds with higher avidity and slower dissociation (36), and subsequent recruitment of additional interactions (37). Although determining the mechanism(s) for stabilization requires further studies, a multi-step binding model can be proposed. For simplicity, we only consider two-step binding (see Appendix), although multi-step binding can be similarly modeled. In the case of affinity regulation, the first step accounts for the initial low-affinity (K_{a1}) binding, and the second step gives rise to the high affinity (K_{a2}) binding. The avidity regulation case can also be treated as a two-step process, with the first step being the formation of a monomeric bond and the second step being the formation of a dimeric bond. For the recruitment case, the first step binding triggers signaling, which results in subsequent recruitment of additional adhesion molecules that bind in the second step. The adhesion probability in the first two cases is given by Eq. 1d and the overall propensity for binding is given by $K_{a1}(1 + K_{a2})$. The only difference for the third case is that K_{a2} in Eq. 1d should be replaced by $m_{r2}m_{l2}A_cK_{a2}$ to account for the mass action effect of the additional molecular species recruited in the second step. The above discussion suggests the following expression for the mean rosette size:

$$\langle n\rangle = \begin{cases} m_rm_lA_cK_{a1}(1 + K_{a2})\eta N & \text{for affinity or avidity upregulation} \\ m_{r1}m_{l1}A_cK_{a1}(1 + m_{r2}m_{l2}A_cK_{a2})\eta N & \text{for subsequent recruitment} \end{cases}, \quad (6)$$

where η ($0 < \eta \leq 1$) denotes the fraction of weak bonds that undergoes stabilization.

This stabilization model is supported by three lines of evidence. First, the observed rosettes require specific receptor-ligand interaction as shown by the control experiments (Fig. 4). Without the specific receptor-ligand binding (which might occur only in the initial phase), stabilization could not produce the Poisson distribution of rosette sizes. Second, the affinities evaluated from fitting the rosette size distributions with our model change when the interacting molecules are changed, indicating their specificity. These data also rule out the multi-species model (the adhesion probability of which is given by Eq. 1c). More significantly, they correlate with the K_a·s of these interactions measured from separate experiments (see above). Third, the Poisson distribution of the rosette size shifts in response to the changes in the receptor and ligand densities in a manner predicted by our model (Fig. 5). Since the model has only a single parameter of mean rosette size, the $\langle n\rangle/m_rm_l$ value does not change with changing m_r and m_l (Fig. 7 *b*). So this value must be proportional, although it may not be equal, to the affinity of the initial interaction K_{a1}. Equation 6 suggests an expression for the constant of proportionality, which is $A_c(1 + K_{a2})\eta N$ or $A_c(1 + m_{r2}m_{l2}A_cK_{a2})\eta N$ depending on the mechanism and fraction of stabilization.

The above discussion also reveals the limitation of using a single binding constant to define the equilibrium between the forward and reverse reaction of receptor-ligand interaction. Indeed, the concept of binding affinity is a useful but often overly simplified model borrowed from the description of chemical bonds at the atomic level. Although this concept has successfully described many receptor-ligand binding data obtained under given experimental conditions, comparison between affinities measured by different experiments using different techniques over different timescales remains a very challenging task. For this reason, the values estimated from the rosette size distribution should be referred to as ''apparent'' effective 2D binding affinities.

In conclusion, a probabilistic model for rosette formation has been developed, which has enabled us to quantitatively relate the rosette size distribution or rosette fraction to the densities of receptors and ligands, their apparent binding affinity, the contact area, and the maximum rosette size. The theoretical prediction compared well with the experimental data for all the cellular and molecular systems examined. The apparent binding affinities so evaluated were consistent with their values determined from other kinetic assays. The insights obtained from this work may be applicable to quantitative understanding of other receptor-ligand interaction-mediated cell-cell adhesion processes.

APPENDIX: STEADY-STATE SOLUTION TO A TWO-STEP BINDING MODEL

Consider a two-step reaction of a receptor (R) binding to a ligand (L):

$$R + L \underset{k_{-1}}{\overset{k_{+1}}{\rightleftharpoons}} (RL)_1 \underset{k_{-2}}{\overset{k_{+2}}{\rightleftharpoons}} (RL)_2. \tag{A1}$$

Here k_{+1} (in $\mu m^{-2}\cdot s^{-1}$) is the rate constant of the first-step second-order association process, and k_{-1}, k_{+2}, and k_{-2} (all in s^{-1}) are the respective rate constants of the first-step dissociation, second-step association, and second-step dissociation processes, respectively, all of which are first-order. Let p_{n_1,n_2} be the probability for the system to be the state (n_1,n_2), i.e., having n_1 $(RL)_1$ bonds and n_2 $(RL)_2$ bonds. Since bond formation and breakage are assumed to be Markovian process, the rate of change of p_{n_1,n_2} in time t depends only on the probabilities of the state (n_1,n_2) and its four intermediate neighbors (n_1-1,n_2), (n_1+1,n_2), (n_1+1,n_2-1), and $(n_1\text{-}1,n_2+1)$, which is governed by the following master equations,

$$\begin{aligned}\frac{dp_{n_1,n_2}}{dt} &= m_r m_l A_c k_{+1} p_{n_1-1,n_2} + (n_1+1)k_{-1}p_{n_1+1,n_2} \\ &\quad + (n_1+1)k_{+2}p_{n_1+1,n_2-1} + (n_2+1)k_{-2}p_{n_1-1,n_2+1} \\ &\quad - [m_r m_l A_c k_{+1} + (k_{-1}+k_{+2})n_1 + k_{-2}n_2]p_{n_1,n_2},\end{aligned} \tag{A2}$$

where A_c is contact area (in unit of μm^{-2}). The kinetic rates are assumed independent of n_1 and n_2 and the number of bonds is assumed to be much smaller than the number of molecules in contact area. In the rosetting experiments, the probabilities should have achieved the steady state, such that the left-hand side of Eq. A2 becomes zero. In addition, the detailed balance between $(RL)_1$ bonds and $(RL)_2$ bonds at equilibrium requires

$$(n_2+1)k_{-2}p_{n_1,n_2+1} = (n_1+1)k_{+2}p_{n_1+1,n_2}. \tag{A3}$$

Upon substitution of Eq. A3, the steady-state equation is simplified as

$$\begin{aligned}m_r m_l A_c k_{+1} p_{n_1-1,n_2} + (n_1+1)k_{-1}p_{n_1+1,n_2} \\ - (m_r m_l A_c k_{+1} + k_{-1}n_1)p_{n_1,n_2} = 0.\end{aligned} \tag{A4}$$

The solution to Eq. A4 can be solved by mathematical induction. Assume the general solution is of the form:

$$\begin{aligned}p_{n_1,n_2} &= \frac{(m_r m_l A_c K_{a1})^{n_1}}{n_1!}\frac{(m_r m_l A_c K_{a1} K_{a2})^{n_2}}{n_2!} \\ &\quad \times \exp[-m_r m_l A_c K_{a1}(1+K_{a2})],\end{aligned} \tag{A5}$$

where $K_{ai} = k_{+i}/k_{-i}$ $(i = 1, 2)$ is the binding affinity of the ith step. It is readily verifiable that this solution satisfies Eq. A3. Equation A5 is true for the case of $n_1 = n_2 = 0$:

$$p_{0,0} = \exp[-m_r m_l A_c K_{a1}(1+K_{a2})], \tag{A6}$$

because this expression has been chosen to allow Eq. A5 to satisfy the normalization condition, $\sum_{n_1=0,n_2=0}^{\infty} p_{n_1 n_2} = 1$. Since $p_{-1,n_2} = 0$, setting $n_1 = n_2 = 0$ in Eq. A4 verifies that Eq. A5 is true for the case of $n_1 = 1$ and $n_2 = 0$:

$$p_{1,0} = m_r m_l A_c K_{a1} p_{0,0} = m_r m_l A_c K_{a1} \exp[-m_r m_l A_c K_{a1}(1+K_{a2})]. \tag{A7}$$

Suppose Eq. A5 holds for $n_1 = n$ and $n_1 = n-1$ $(n > 1)$. Substituting these assumed solutions for p_{n,n_2} and p_{n-1,n_2}into Eq. A4 yields

$$\begin{aligned}p_{n+1,n_2} &= \frac{1}{(n+1)k_{-1}}[(m_r m_l A_c k_{+1} + k_{-1}n)p_{n,n_2} \\ &\quad - m_r m_l A_c k_{+1} p_{n-1,n_2}] \\ &= \frac{(m_r m_l A_c K_{a1})^{n+1}}{(n+1)!}\frac{(m_r m_l A_c K_{a1} K_{a2})^{n_2}}{n_2!} \\ &\quad \times \exp[-m_r m_l A_c K_{a1}(1+K_{a2})].\end{aligned} \tag{A8}$$

Thus, Eq. A5 is shown to be true for $n_1 = n+1$. Although Eq. A5 has only been shown for the case of $n_2 = 0$ (Eqs. A6 and A7), the derivation of Eq. A8 does not require the specification of n_2. In addition, the solution for the $n_2 > 0$ case can be easily generated from that for the $n_2 = 0$ case using Eq. A3. For example, setting $n_1 = n_2 = 0$ in Eq. A3 and using Eqs. A6 and A7 result in

$$p_{0,1} = K_{a2} p_{1,0} = m_r m_l A_c K_{a1} K_{a2} \exp[-m_r m_l A_c K_{a1}(1+K_{a2})], \tag{A9}$$

verifying that Eq. A5 is also true for the case of $n_1 = 0$ and $n_2 = 1$. It thus follows from the principle of mathematical induction that Eq. A4 is true for any nonnegative n_1 and n_2 values. The adhesion probability, P_a, can be easily obtained from Eq. A6:

$$P_a = 1 - p_{0,0} = 1 - \exp[-A_c m_r m_l K_{a1}(1+K_{a2})]. \tag{A10}$$

We thank Dr. T. K. Kishimoto for the generous gifts of the L-selectin construct and the DREG56 and CA21 mAbs, and Dr. S. Sambhara for providing spleens of F5 transgenic mouse. We also thank E. Moses and J. Plowden for technical assistance, and J. Huang for protein coating and flow cytometry assays. We thank the NIH Tetramer Facility for providing pMHC monomers.

This work was supported by National Natural Science Foundation of China grants 10332060, 30225027, and 10128205; a Chinese Academy of Sciences grant KJCX2-SW-L06 (M.L.); and NIH grants AI44902 and AI38282 (C.Z.), TW 05774-01 (C.Z. and M.L.), HL 65631 (R.P.M.), and AI49400 (P.S.).

REFERENCES

1. Selvaraj, P., M. L. Plunkett, M. L. Dustin, M. E. Sanders, S. Shaw, and T. A. Springer. 1987. The T-lymphocyte glycoprotein CD2 binds the cell surface ligand LFA-3. *Nature*. 326:400–403.
2. Springer, T. A. 1990. Adhesion receptors of the immune system. *Nature*. 346:425–434.
3. Selvaraj, P., M. L. Dustin, R. Mitnacht, T. Hunig, T. A. Springer, and M. L. Plunkett. 1987. Rosetting of human T lymphocytes with sheep and human erythrocytes. Comparison of human and sheep ligand binding using purified E receptor. *J. Immunol.* 139:2690–2695.
4. Nagarajan, S., S. E. Chesla, L. Cobern, P. Anderson, C. Zhu, and P. Selvaraj. 1995. Ligand binding and phagocytosis by CD16 (Fcγ receptor III) isoforms. Phagocytic signaling by associated ζ and γ subunits in Chinese hamster ovary cells. *J. Biol. Chem.* 270:25762–25770.
5. Nagarajan, S., S. E. Chesla, L. Cobern, P. Anderson, C. Zhu, and P. Selvaraj. 2000. Cell-specific, activation-dependent regulation of neutrophil CD32A ligand-binding function. *Blood*. 270:25762–25770.
6. Brown, R. A., R. C. Potts, A. J. Robertson, P. C. Hayes, K. Ramesar, and J. Swanson Beck. 1979. A new method for semi-automated quantitation of E-rosettes using a particle size analyzer (Coulter channel analyzer). *J. Immunol. Methods*. 24:117–131.
7. Perelson, A. S. 1985. A model for antibody mediated cell aggregation: rosette formation. *In* Mathematics and Computers in Biomedical Applications. J. Bisenfeld and C. DoLisl, editors. Elsevier Science Publishers B.V., North-Holland. 31–37.
8. Piper, J. W., R. A. Swerlick, and C. Zhu. 1998. Determining force dependence of two-dimensional receptor-ligand binding affinity by centrifugation. *Biophys. J.* 74:492–513.
9. Chesla, S. E., P. Selvaraj, and C. Zhu. 1998. Measuring two-dimensional receptor- ligand binding kinetics by micropipette. *Biophys. J.* 75:1553–1572.
10. Long, M., H. L. Goldsmith, D. F. J. Tees, and C. Zhu. 1999. Probabilistic modeling of shear-induced formation and breakage of doublets cross linked by receptor–ligand bonds. *Biophys. J.* 76:1112–1128.
11. Zhu, C., and T. E. Williams. 2000. Modeling concurrent binding of multiple molecular species in cell adhesion. *Biophys. J.* 79:1850–1857.
12. Zhu, C. 2000. The kinetics and mechanics of cell adhesion. *J. Biomech.* 33:23–33.
13. Williams, T. E., P. Selvaraj, and C. Zhu. 2000. Concurrent binding to multiple ligands: kinetic rates of CD16b for membrane-bound IgG1 and IgG2. *Biophys. J.* 79:1858–1866.
14. Williams, T. E., S. Nagarajan, P. Selvaraj, and C. Zhu. 2000. Concurrent and independent binding of Fcγ receptors IIa and IIIb to surface-bound IgG. *Biophys. J.* 79:1867–1875.
15. Williams, T. E., S. Nagarajan, P. Selvaraj, and C. Zhu. 2001. Quantifying the impact of membrane microtopology on effective two-dimensional affinity. *J. Biol. Chem.* 276:13283–13288.
16. Zhu, C., M. Long, S. E. Chesla, and P. Bongrand. 2002. Measuring receptor/ligand interaction at the single-bond level: Experimental and interpretative issues. *Ann. Biomed. Eng.* 30:305–314.
17. Huang, J., J. Chen, S. E. Chesla, T. Yago, P. Mehta, R. P. McEver, C. Zhu, and M. Long. 2004. Quantifying the effects of molecular orientation and length on two-dimensional receptor-ligand binding kinetics. *J. Biol. Chem.* 279:44915–44923.
18. Dumaswala, U. J., M. J. Wilson, T. Jose, and D. L. Daleke. 1996. Glutamine- and phosphate-containing hypotonic storage media better maintain erythrocyte membrane physical properties. *Blood*. 88:697–704.
19. Selvaraj, P., W. F. Rosse, R. Silber, and T. A. Springer. 1988. The major Fc receptor in blood has a phosphatidylinositol anchor and is deficient in paroxysmal nocturnal hemoglobinuria. *Nature*. 333:565–567.
20. Ushiyama, S., T. M. Laue, K. L. Moore, H. P. Erickon, and R. P. McEver. 1993. Structural and functional characterization of monomeric soluble P-selectin and comparison with membrane P-selectin. *J. Biol. Chem.* 268:15229–15237.
21. Geng, J. G., M. P. Bevilacqua, K. L. Moore, T. M. McIntyre, S. M. Prescott, J. M. Kim, G. A. Bliss, G. A. Zimmerman, and R. P. McEver. 1990. Rapid neutrophil adhesion to activated endothelium mediated by GMP-140. *Nature (Lond.)*. 343:757–760.
22. Moore, K. L., K. D. Patel, R. E. Bruehl, F. Li, D. A. Johnson, H. S. Lichenstein, R. D. Cummings, D. F. Bainton, and R. P. McEver. 1995. P-selectin glycoprotein ligand-1 mediates rolling of human neutrophils on P-selectin. *J. Cell Biol.* 128:661–671.
23. Kahn, J., R. H. Ingraham, F. Shirley, G. I. Migaki, and T. K. Kishimoto. 1994. Membrane proximal cleavage of L-selectin: Identification of the cleavage site and a 6-kD transmembrane peptide fragment of L-selectin. *J. Cell Biol.* 125:461–470.
24. Kishimoto, T. K., M. A. Jutila, and E. C. Butcher. 1990. Identification of a human peripheral lymph node homing receptor: a rapidly down-regulated adhesion molecule. *Proc. Natl. Acad. Sci. USA*. 87:2244–2248.
25. Mamalaki, C., T. Norton, Y. Tanaka, A. R. Townsend, P. Chandler, E. Simpson, and D. Kioussis. 1992. Thymic depletion and peripheral activation of class I major histocompatibility complex-restricted T cells by soluble peptide in T-cell receptor transgenic mice. *Proc. Natl. Acad. Sci. USA*. 89:11342–11346.
26. Kofler, R., and G. Wick. 1977. Some methodologic aspects of the chromium chloride method for coupling antigen to erythrocytes. *J. Immunol. Methods*. 16:201–209.
27. McQuarrie, D. A. 1963. Kinetics of small systems. I. *J. Chem. Phys.* 38:433–436.
28. Li, P., P. Selvaraj, and C. Zhu. 1999. Analysis of competition binding between soluble and membrane-bound ligands for cell surface receptors. *Biophys. J.* 77:3394–3406.
29. Chesla, S. E., P. Li, S. Nagarajan, P. Selvaraj, and C. Zhu. 2000. The membrane anchor influences ligand binding 2D kinetics rates and 3D affinity of FcγRIII (CD16). *J. Biol. Chem.* 275:10235–10246.
30. Long, M., H. Zhao, K. S. Huang, and C. Zhu. 2001. Kinetic measurements of cell surface E-selectin/carbohydrate ligand interactions. *Ann. Biomed. Eng.* 29:935–946.
31. Zhang, F., W. D. Marcus, N. F. Goyal, S. Selvaraj, T. A. Springer, and C. Zhu. 2005. Two-dimensional kinetics regulation of $\alpha_L\beta_2$-ICAM-1 interaction by conformational changes of the α_L inserted domain. *J. Biol. Chem.* 280:42207–42218.
32. Marshall, B. T., M. Long, J. W. Piper, T. Yago, R. P. McEver, and C. Zhu. 2003. Direct observation of catch bonds involving cell-adhesion molecules. *Nature*. 423:190–193.
33. Sarangapani, K. K., T. Yago, A. G. Klopocki, M. B. Lawrence, C. B. Fieger, S. D. Rosen, R. P. McEver, and C. Zhu. 2004. Low force decelerates L-selectin dissociation from P-selectin glycoprotein ligand-1 and endoglycan. *J. Biol. Chem.* 279:2291–2298.
34. Jiang, N. 2005. Kinetic studies of Fcγ receptor III and T cell receptor. PhD thesis. Georgia Institute of Technology, Atlanta, GA.
35. Li, S. H., D. K. Burns, J. M. Rumberger, D. H. Presky, V. L. Wilkinson, M. Anostario Jr., B. A. Wolitzky, C. R. Norton, P. C. Familletti, and K. J. Kim. 1994. Consensus repeat domains of E-selectin enhance ligand binding. *J. Biol. Chem.* 269:4431–4437.
36. Carman, C. V., and T. A. Springer. 2003. Integrin avidity regulation: are changes in affinity and conformation underemphasized? *Curr. Opin. Cell Biol.* 15:547–556.
37. Bazzoni, G., and M. E. Hemler. 1998. Are changes in integrin affinity and conformation overemphasized? *Trends Biochem. Sci.* 23:30–34.